Food Innovation and Advances

ARTICLE

Open Access

https://doi.org/10.48130/fia-0025-0004

Food Innovation and Advances **2025**, 4(1): 1–9

Back Propagation Neural Network model for analysis of hyperspectral images to predict apple firmness

Shuiping Li[1], Yueyue Chen[1], Xiaobo Zhang[2], Junbo Wang[3], Xuanxiang Gao[1], Yunhong Jiang[4], Zhaojun Ban[1*] and Cunkun Chen[5*]

[1] *School of Biological and Chemical Engineering, Zhejiang University of Science and Technology, Zhejiang Provincial Key Laboratory of Chemical and Biological Processing Technology of Farm Products, Zhejiang Provincial Collaborative Innovation Center of Agricultural Biological Resources Biochemical Manufacturing, Hangzhou 310023, China*

[2] *Computer of Science and Technology, Huazhong University of Science and Technology, Wuhan 430074, China*

[3] *Aksu Youneng Agricultural Technology Co., Ltd, Aksu 843001, China*

[4] *Department of Applied Sciences, Faculty of Health and Life Science, Northumbria University, Newcastle Upon Tyne, NE1 8ST, United Kingdom*

[5] *Institute of Agricultural Products Preservation and Processing Technology (National Engineering Technology Research Center for Preservation of Agriculture Product), Tianjin Academy of Agricultural Sciences; Key Laboratory of Postharvest Physiology and Storage of Agricultural Products, Ministry of Agriculture and Rural Affairs of P.R.China, Tianjin 300384, China*

* Corresponding authors, E-mail: banzhaojun@zust.edu.cn; cck0318@126.com

Abstract

The potential of employing hyperspectral imaging (HSI) in the near-infrared (NIR) range (386.82–1,004.50 nm) for predicting the firmness of 'Fuji' apples cultivated in Aksu has been evaluated. The performance of seven preprocessing algorithms and two feature selection algorithms was evaluated. The coefficient of determination (R^2) and root mean square error (RMSE) of Partial Least Squares (PLS) models are contrasted using various inputs. These results confirm that the Multiplicative Scatter Correction (MSC) preprocessing algorithm was the optimal choice (R_p^2 = 0.7925, *RMSEP* = 0.6537), and the Competitive Adaptive Reweighted Sampling (CARS) feature selection algorithm demonstrated superior performance (R_p^2 = 0.8325, *RMSEP* = 0.6257). Based on the aforementioned findings, PLS, Multiple Linear Regression (MLR), Heterogeneous Transfer Learning (HTL), and Back Propagation Neural Network (BPNN) models were constructed for cross-validation purposes. The experimental results indicate that the CARS-BPNN model exhibits the optimal prediction performance, with an R_p^2 value of 0.9350 and an *RMSEP* value of 0.4654. The results of the research indicated that a deep learning method combined with hyperspectral imaging technology could be utilized to non-destructively detect the firmness of 'Fuji' apples, which will be beneficial and potentially applicable for post-harvest fruit firmness monitoring. This research provides a reference point for the non-destructive detection of apple in the selection of preprocessing, feature selection algorithms, and predicting firmness model.

Citation: Li S, Chen Y, Zhang X, Wang J, Gao X, et al. 2025. Back Propagation Neural Network model for analysis of hyperspectral images to predict apple firmness. *Food Innovation and Advances* 4(1): 1–9 https://doi.org/10.48130/fia-0025-0004

Introduction

China holds a dominant position in the world's apple production, having the greatest apple-growing area, and the largest export[1]. Apples' rich trace elements and organic component composition give them a delicious flavor and significant nutritional benefits. In this case, the quality of apples has a significant impact by several factors, including shape, size, sugar, acids, external colour, soluble solids content (SSC), and texture[2]. However, weight loss, disease, and chilling injury of postharvest loss are the most common occurrences. These losses may affect customer purchasing decisions and result in a decline in apple sales[3]. Detecting all postharvest loss parameters is unquestionably intricate. Research has revealed a substantial link between fruit weight reduction and texture attributes, suggesting that texture trait evaluations may be used to determine postharvest loss[4].

Firmness is an important metric for analyzing textural characteristics and determining the degree of postharvest loss. At present, the techniques employed for determining firmness are largely based on conventional physicochemical methods, and sensory analysis. However, these approaches are known to be detrimental, time-consuming, and arduous[5]. The industry standard for determining the firmness of fruits is a penetrometer test that involves piercing fruit flesh to a depth with a Magness-Taylor instrument, which leads to a loss of financial losses[6]. Hence, it is essential to develop a rapid, non-destructive test technique for monitoring apple firmness.

Several research works have been carried out non-destructive evaluation of fruit quality using acoustic[7], multispectral imaging[8], hyperspectral imaging[9], electronic nose[10], fluorescence imaging[11], machine vision[12], and so on. Hyperspectral imaging stands out as the most comprehensive of the approaches listed above since it allows for the utilization of both visual and spectral data from the sample for firmness detection[13]. The mechanism behind some detections is grounded on the measurement of the spectrum from the fruit surface by reflection, interaction, or transmission. By applying certain chemometric techniques, the relevant wavelength variations in the spectrum can be employed to be connected with firmness, because the measured spectrum is related to the content and structure of the fruit[14].

However, because hyperspectral imaging remains enormously dimensional, standard processing techniques find it challenging to handle the massive volume of data. In this project, we intend to introduce deep learning techniques. Using huge amounts of data or high dimensional data, deep learning creates deep neural networks to simulate human brain neurons and perform complicated function approximation[15]. With numerous successful applications in the fields of food, image processing, speech recognition, and object detection, these techniques have demonstrated their sophisticated

technology for big data analysis[16]. More studies on the hyperspectral imaging for fruit quality assessment could be found such as loquat[17], apple[18], kiwifruit[19], blueberry[20], and banana[21]. Xiang et al.[22] completed SSC and firmness nondestructive testing of tomatoes, applying hyperspectral imaging and deep learning. Additionally, a novel regression model based on one-dimensional (1D) Con1dResNet (Con1dResNet) was proposed and evaluated in comparison to existing techniques. The evaluation results indicate that with a sufficiently large number of samples, this technique outperforms the state-of-the-art technique by 26.4% for SSC and 33.7% for firmness[22]. Hyperspectral imaging and deep learning were utilized by Xu et al. to predict the firmness and pH of Kyoho grapes[23]. Their research demonstrated that grape firmness and acidity may be rapidly and non-destructively assessed through the integration of stacked auto-encoders (SAE) with hyperspectral imaging. At the moment, the majority of literature researches concentrate on optimization of a single model, which results in a lack of comparison effect of other models and limited reference value.

This manuscript's particular goals were: (1) Process the spectral data and firmness indicators of the collected apple samples in order to determine the optimal spectral preprocessing method; (2) Compare the optimization of feature wavelength extraction methods in order to determine the optimization feature wavelength extraction methods; (3) Optimization learn modeling by selecting methods: multiple linear regression (MLR), heterogeneous transfer learning (HTL), and backpropagation neural network (BPNN); (4) Through various modeling analysis and prediction effects on the firmness of apple samples, the modeling method with a larger coefficient of determination (R^2) and a smaller root mean squared error (*RMSE*) is selected to determine the best prediction model to achieve the optimal result for apple firmness.

Materials and methods

Apple material

All the 220 tested apples (*Malus domestica* Borkh) were harvested on local farms (80°20' E, 41°28' N, Aksu Prefecture, Xinjiang, China) within a week after the frost's descent (25–30 October, 2023). The average apple weight of these apple samples was 233.42 g and the average apple diameter was 83.40 mm. After removing the frost wax, the apple samples were numbered and labeled. Following that, spectral analysis and associated experiments were used to analyze the apple samples. The raw data set was rearranged at a 4:1 ratio using the Kennard-Stone algorithm (KS), resulting in the generation of two distinct datasets: a calibration set comprising 176 apple samples and a prediction set comprising 44 apple samples.

Hyperspectral image

In the actual screening process, the position of the apple is not fixed and there are numerous potential configurations. To enhance the precision of detection, we opted to gather four surfaces of apples in a flat position, aiming to gather as much surface information as feasible. The experiment used a push-and-scan hyperspectral imaging camera (ResononPikaKC2 imaging spectrometer, Beijing Liga, Beijing, China), linear mobile platform, installation tower, lighting device, head, NB single-phase current intelligent detector, GST36U12-P1JW power supply sensor (Mingwei, Taiwan), DMX-J-SA-17 stepper motor (Arcas, USA), acA1920-155 μm array camera (Basler, Germany). The hyperspectral spectrometer included an exposure time of 20.0 ms, a frame frequency of 20.0 HZ, a spectral resolution of 1.3 nm, and a spectral range of 386.82–1,004.50 nm. The platform has a maximum operating rate of 355 pps (packets per second), a maximum gain of 3, and a fixed distance of 20.0 cm between the sample and the camera[24].

Firmness measurement

Firmness measurement using GY-1 fruit firmness tester (Dongguan Sanliang Measuring Tools Co., Ltd, Dongguan, China), suitable for measuring apples, pears, and other high-firmness fruits professionally. The scale display range is 2–15 kg/cm^2, the side head diameter size is 3.5 mm, the index value is 0.1 kg/cm^2, and the indentation depth of the indenter is standardized to 10 mm. The external dimensions of the firmness tester are 140 mm × 60 mm × 30 mm and the net weight is 0.5 kg. Considering that the GY-1 firmness tester is a manual measurement, to ensure the accuracy of the experiment, apple samples need to be collected three times the firmness value, and take the average of the three as the final firmness of the sample to obtain the measurement value. The final experimental solution was determined as three different parts of the apple on the equatorial line, with each part spaced 120 degrees apart.

Spectral data extraction

In order to obtain a stable light environment, the hyperspectral imaging equipment should be turned on and warmed up for approximately half an hour before scanning each sample. By using Eqn (1), the raw hyperspectral image is calibrated with the standard white and dark reference images in order to remove the effects of uneven illumination and dark current noise[25].

$$R_c = (R_0 - B)/(W - B) \quad (1)$$

In this context, R_c represents the calibrated hyperspectral image, R_0 designates the raw hyperspectral data, W means the standard white reference image obtained through the use of a rectangular Teflon plate, and B stands for the standard black reference image, which is obtained by fully covering the lens completely with an opaque black cover.

Every apple was given a hyperspectral image, which was then preprocessed and used to extract the spectra. To extract the spectral data information from the acquired spectral image of the apple sample, a 150 × 150 pixels region of interest (ROI) was identified in the vicinity of the equatorial plane. The Environment for Visualizing Images software (ENVI 5.1, Research Systems Inc, Boulder, CO, USA) was used to calculate the raw average reflectance from ROI.

Spectral processing

Spectral preprocessing can boost accuracy, remove redundant and erroneous information, and lessen the impact of light, noise, and background interference produced by the test instrument during the spectrum acquisition procedure on the measured light spectrum data. To reduce noise from various electronic sources and variations in sample conditions, the raw mean spectra data were preprocessed using seven standard methods: Min Max Scaler (MMS)[26], Standard Scaler (SS)[27], Mean Centering (CT)[28], Standard Normal Variate (SNV)[29], Moving Average (MA)[30], Savitzky Golay smoothing filtering (SG)[31], and Multiplicative Scatter Correction (MSC)[32].

The Partial least squares regression (PLS) model was developed using the pre-treated spectrum and the raw spectrum, with the determination coefficient (R^2) and the root mean square error (*RMSE*) as the evaluation indexes, and the optimal scheme was determined by selecting the one with greater R^2 and a smaller *RMSE*. The calculation formulas of R^2 and *RMSE* are shown in Eqns (2) & (3):

$$R_c^2, R_p^2 = 1 - [\sum_{i=1}^{n}(y_i - \hat{y}_i)^2 / \sum_{i=1}^{n}(y_i - y_m)^2] \quad (2)$$

$$RMSEC,\ RMSEP = \sqrt{\frac{1}{n}\sum_{i=1}^{n}(y_i - y_m)^2} \quad (3)$$

where, $\hat{y}_i$ express the predicted value of the i^{th} sample, y_i means the measured value of the i^{th} sample, n shows the total number of samples, and y_m is the mean value of the samples.

Feature selection algorithm

The selection of an effective wavelength is a crucial aspect of spectral data analysis. Its function is to eliminate superfluous information present in the spectrum, retain data pertinent to the current task, and subsequently reduce the data dimension[33]. The Competitive Adaptive Reweighted Sampling (CARS) algorithm enables the identification of the optimal combination of specific key variables, thereby enhancing the detection of corresponding indicators[34]. The Random Frog (RF) algorithm is employed to find the most likely significant variables, then local search is used to expand the significant variable interval width[35]. At present, there are successful cases of the application of CARS and RF in combining the firmness of hyperspectral technology. Both feature wavelength selection algorithms have certain superiority. Based on a comprehensive consideration of the article, we have selected the above two feature selection methods for experimental investigation.

CARS not only optimizes the accuracy of firmness prediction but also increases the efficiency of the prediction model in comparison to other feature wavelength selection algorithms, including the Successive Projection Algorithm (SPA)[36], and Principal Component Analysis (PCA)[37]. It chooses the wavelengths exhibiting the greatest absolute values of the PLS model's regression coefficients, emulating the Darwinian principle of 'survival of the fittest'[38]. CARS is capable of filtering out the most complex bands with the greatest number of eigenvalues, and can be combined with other processing methods to enhance the accuracy and stability of the model[39]. Experiments have been conducted to establish a correlation between hyperspectral images and kiwifruit hardness, with successful results in predicting and visualizing this variable. Therefore, the use of CARS is both reasonable and appropriate for the experiment[40].

The PLS model was created by the algorithm using 80% randomly divided data sets for analysis. The target variable's explanatory value is determined by the regression coefficient's absolute value. Every sample iteration involves four sequential steps that CARS goes through to function: (1) Model sampling using Monte Carlo; (2) Perform enforced wavelength selection, using an exponentially diminishing function; (3) Adopt ARS to achieve a competitive wavelength selection process; (4) Use cross-validation to assess the subset[41]. In this study, the Monte Carlo sampling run times were 500, the maximum principal component number was 10, the sampling rate was 0.8, and the optimal number of iteration number was 195. Equations (4)–(6) describe the most important theory of CARS.

$$r_i = \alpha e^{-ki} \tag{4}$$

$$\alpha = (P/2)^{1/(N-1)} \tag{5}$$

$$k = \ln(P/2)/(N-1) \tag{6}$$

where, r_i shows the ratio column of reserved wavelength points obtained, i express the Monte Carlo sampling runs, α and k are two constants, P designates the raw wavelength number, N means preset Monte Carlo sampling number.

The RF algorithm is based on post-heuristic particle swarm optimization, enabling the iterative process by integrating the benefits of the reversible jump Markov chain Monte Carlo algorithm. The selection probability of the variable is calculated using the Markov chain based on the stationary distribution. The optimal bands selected by RF provide a technical foundation for subsequent semi-quantitative modeling of spectroscopy and chemometrics[42]. In light of the possibility of errors in the CARS (ignoring interactions between features or errors caused by other reasons), the CARS algorithm is used to extract features while the RF algorithm is used to select spectral features[43]. There are four steps in the process: (1) Set the initial number of frog population variables Q, which form a subset V_0; (2) Calculate the positional fitness of each variable; (3) Appropriately transform the frog position according to its fitness and relevance to the problem; (4) After N iterations, calculate the probability of the variable being selected according to Eqn (7)[35]. The RF algorithm had its operational specifications set as follows: the number of iterations N was 3000, the frog population variables Q was 6, and the resampling factor for variable adjustment was 10.

$$Probability_i = N_j/N, \qquad j = 1,2,3,\ldots,p \tag{7}$$

where, $Probability_i$ designates the probability variables, N_i means iterations number in progress, N is the total iterations number, p expresses the total wavelength number.

Firmness prediction models

To create models between the apple's firmness and feature wavelength, four common techniques were used: Back Propagation Neural Network (BPNN), Heterogeneous Transfer Learning (HTL), Multiple Linear Regression (MLR), and PLS. Supervised learning in hyperspectral imaging analysis frequently uses methods like MLR. Because it can identify the linear relationships with a single independent variable and a multitude of dependent variables.

The objective of MLR is to minimize the discrepancies between anticipated and actual results by using a simple method of assigning values to the independent variable coefficients[44]. The majority of HTL techniques used today deal with heterogeneous domains by either learning an asymmetric transformation between them or discovering a common subspace for them. The objective is to use knowledge (or information) from related tasks to enhance performance on the target learning task[45].

By using an end-to-end feature extraction method in place of the manual feature extraction process, BPNN may swiftly extract information about hidden features from a given data set[46]. There are different types of layers that make up the structure of a neural net: (1) the input layer, which contains the basic data of the network; (2) the hidden layer, which works as an intermediary between the intermediate input layer and the downstream output layer; and (3) the output layer, which generates the output based on the input.

Following building the regression model, the models were evaluated for accuracy using the determination coefficient of calibration and prediction (R_c^2 and R_p^2) and the root mean square error of calibration and prediction (*RMSEC* and *RMSEP*). Formulas for parametric in the spectral processing section.

Using the characteristic wavelength data elected by CARS and RF, the prediction model of apple firmness based on the MLR algorithm was established. For the network model optimizer of transfer learning, Adaptive Moment Estimation (ADAM) was elected as the network model optimizer for transfer learning; Leaky Rectified Linear Unit (Leaky ReLU) was taken as the activation function; Mean Squared Error (MSE) was chosen as the loss function; Mean Absolute Error (MAE) was chosen as the training evaluation criterion; the batch size was 64; the verification ratio of each round was 0.2; the initial learning rate was 0.0005. The initial training rounds epoch was 20. The value of the output layer represents the predicted firmness, and the number of layers is 1. The number of neurons in the hidden layer is 26, and the training stride is 20000.

Results and discussion

Spectral characteristics

Due to the large amount of physical and chemical information it includes, hyperspectral information is extremely dimensional and collinear. The entire sample spectral (386.82–1,004.50 nm) derived from the hyperspectral image of the apple sample is shown in Fig. 1.

The complete spectral data set, comprising 220 samples, is presented in this figure, where the horizontal coordinates represent the hyperspectral wavelengths and the vertical coordinates indicate the spectral absorbance.

The raw spectral data is divided into bands at approximately 1.32 nm intervals, so all the data is divided into a total of 462 band counts. The spectra of all samples exhibit a similar pattern, with a single peak and three valleys. The peak was observed at 810 and 830 nm, whereas the valleys were observed at 400–600, 690, and 960 nm. It has a peak at 810 and 830 nm is part of the chlorophyll absorption spectra[47].

Statistics of reference firmness

The mean value of 8.97 kg/cm^2 and the standard deviation (SD) of 0.90 kg/cm^2 for all 220 examined apple samples showed a change in firmness from 6.45 to 12.30 kg/cm^2. The samples' largest and lowest values differed by 5.85. The results demonstrate that even in the same origin, the quality of the same batch of fruit still had notable variations, so is essential to establish a non-destructive testing method.

The distribution histogram and firmness box diagram shown in Fig. 2 highlight the fact that most samples cluster in the 8–10 kg/cm^2 range, despite the firmness index parameters having a fairly wide span. For the accuracy and dependability of the predictive model, this concentration is quite beneficial.

Spectral data processing

By removing unnecessary data and reducing the impact of background noise, spectral preprocessing can increase model prediction accuracy. Figure 3 displays seven images of the whole sample by process.

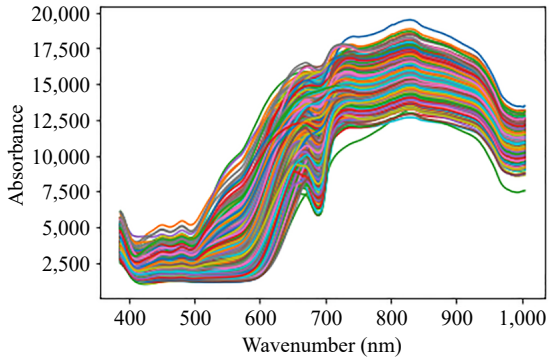

Fig. 1 Sample spectra of apples.

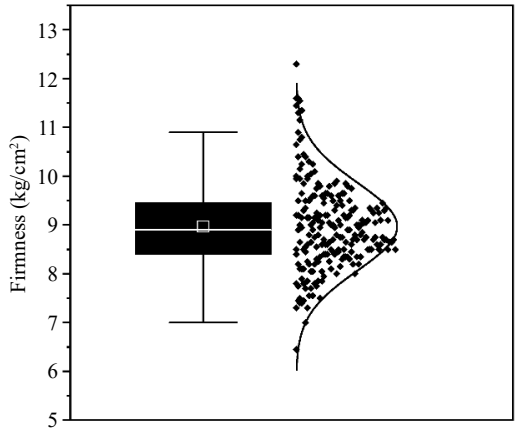

Fig. 2 Boxplot and normal curve plots of firmness.

There is no discernible difference between the other results in the collection of graphs, except the results derived from the MMS and SS algorithms, which call for more investigation and analysis. The spectral images processed by MMS and SS are manifestly more diffuse than the raw, which makes the data smoother but diminishes the correlation and learning potential of the data, and renders it more challenging to construct the prediction model subsequently. The spectral image data obtained from the remaining five processing methods are more centralized, which strengthens the normalization of the data and can effectively promote the learning speed of the prediction model. However, for all the preprocessing methods, it is difficult to illustrate the advantages and disadvantages of the data solely based on the spectral images. Therefore, further analysis and validation are necessary.

The pre-processed spectral wavelength and the raw wavelengths (RW) were employed as input for the establishment of PLS regression models, which were utilized to assess the efficacy of the various processing algorithms. These models facilitated a visual analysis of the performance of the treated spectral data. Table 1 illustrates the potential for information loss and decreased model prediction accuracy caused by the seven spectrum preprocessing techniques (MMS, SS, CT, SNV, MA, SG, and MSC). The preprocessed data will exhibit a modest decrease relative to the original dataset when evaluating training outcomes. This is attributable to the inherent limitations of data processing, which inevitably entail a certain degree of data loss. Consequently, it becomes essential to identify a preprocessing algorithm that approximates the characteristics of the original data set. The *RMSE* of the preprocessing procedures was computed respectively for each type of input data when building a PLS regression model using the data. The model's accuracy and stability increase with decreasing RMSE, but the R_p^2 has the reverse effect. The MSC preprocessing approach has a greater prediction accuracy; the R_p^2 is 0.7925, the *RMSEP* is 0.6537, and R_c^2 and *RMSEC* are 0.7862, 0.6525, respectively. An examination of the data table reveals that the evaluation values of SG and MSC exhibit close alignment with the original data set. Nevertheless, SG exhibits suboptimal performance when applied to the prediction set. Consequently, after weighing these observations, the MSC algorithm is selected as the preprocessing algorithm for the forthcoming experiment.

Feature wavelength selection

Following the segmentation of the raw samples using the KS algorithm and subsequent processing using the MSC algorithm, the feature wavelengths were obtained through the application of the CARS and RF algorithms. CARS and RF algorithms were employed to select feature wavelengths that were connected with the firmness, reducing data redundancy, and increasing model operating efficiency. To determine the suitability of the CARS algorithm for extracting feature wavelengths from pre-processed spectra, the *RMSE* and the R^2 of the model were determined for a range of feature spectral wavelengths. The lower the *RMSE* and the higher the R^2, the greater the precision and reliability of the model. When the RMSE attains a minimum value, the number of wavelengths extracted as features is 13, representing 2.81% of the all-spectral band. As demonstrated in Fig. 4, adaptive reweighted sampling has been applied to select the wavelength with the largest absolute value of the PLS model, and cross-validation modeling was used to identify the subset of optimal wavelength variables. When the spectral data was extracted by CARS features, the number of selected wavelengths also decreased from 462 to 1 as the Monte Carlo sampling number increased from 1 to 350. In this process, the 195th iteration interactive verification error (*RMSECV*) was the smallest, and 13 feature wavelengths were proposed.

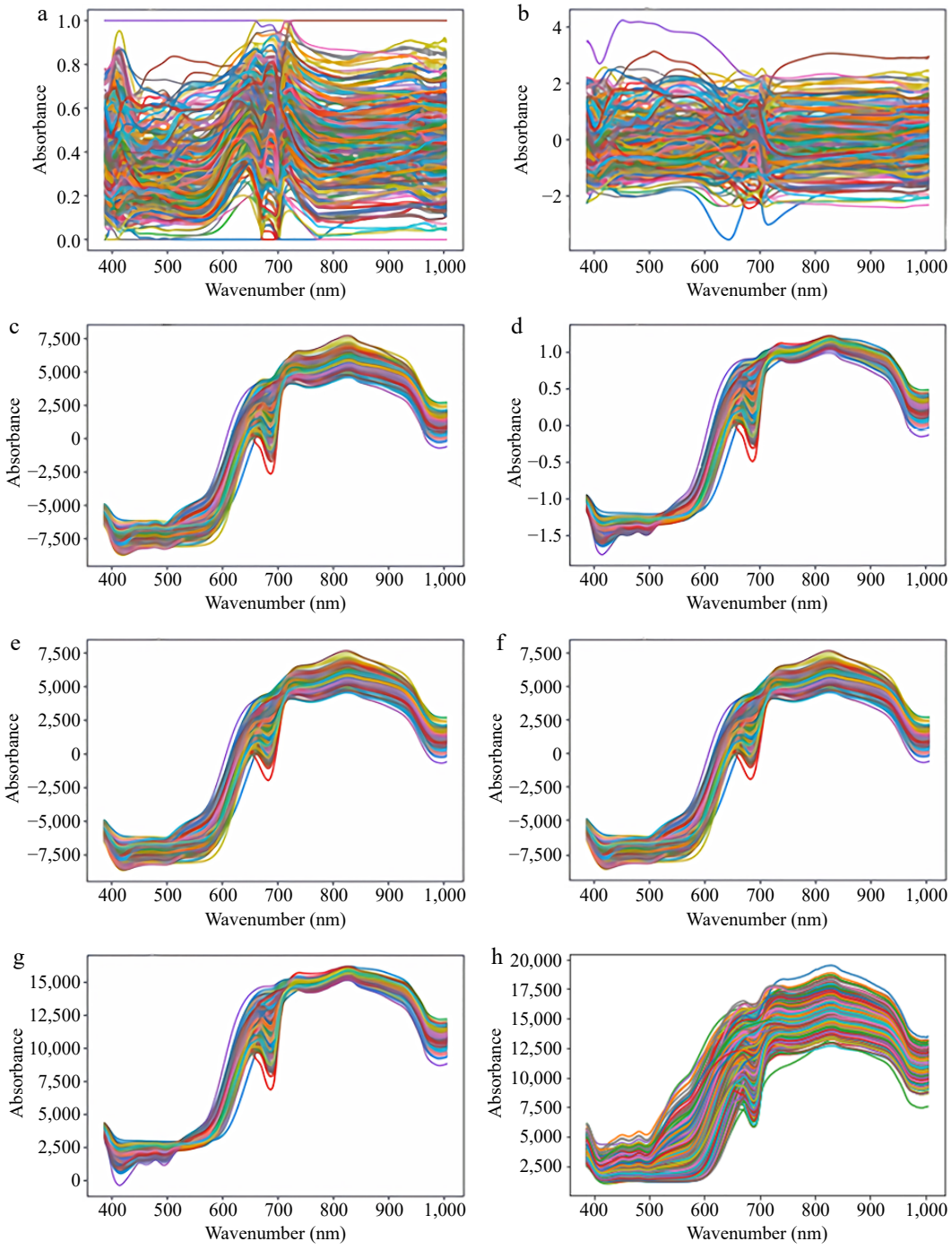

Fig. 3 Wavelength processing graph based on the seven different pre-processing algorithms and the raw wavelength graph. (a) Min Max Scaler, the spectrum of the MMS for dataset, (b) Standard Scaler, the spectrum of the SS for dataset, (c) Mean Centering, the spectrum of the CT for dataset, (d) Standard Normal Variate, the spectrum of the SNV for dataset, (e) Moving Average, the spectrum of the MA for dataset, (f) Savitzky Golay, the spectrum of the SG for dataset, (g) Multiplicative Scatter Correction, the spectrum of the MSC for dataset, (h) Raw Wavelength, the spectrum of the RW for dataset.

Table 1. Comparison of different processing methods in the calibration set and prediction set.

Method	R_c^2	*RMSEC*	R_p^2	*RMSEP*
MMS	0.7247	0.8081	0.7130	0.8330
SS	0.7795	0.6855	0.7690	0.7336
CT	0.7758	0.6935	0.7780	0.7083
SNV	0.7750	0.6993	0.7861	0.6770
MA	0.7876	0.6481	0.6778	0.8902
SG	0.7913	0.6434	0.6680	0.9013
MSC	0.7862	0.6525	0.7925	0.6537
RW	0.7942	0.6357	0.7891	0.6613

Figure 5 shows that the variable's selection probability spans from 0.0 to 0.35, and that the higher the probability of a variable, the bigger the modeling impact. A distinct variable address was linked to every spectral wavelength. Characteristic wavelength variables are those wavelengths that have an associated variable with a selection probability above 0.132. Finally, the number of selected bands in this interval is 17. The selection probability value of variables in these wavelength ranges is high, which indicates that these wavelengths also have a stronger influence on modeling.

The majority of feature wavelength selection algorithms markedly diminish the overall complexity of variables while maintaining a

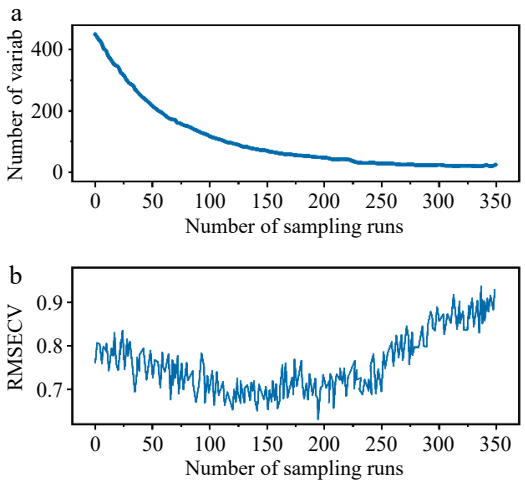

Fig. 4 Firmness feature extraction of CARS. Trend charts of (a) selecting the number of wavelengths and (b) RMSECV.

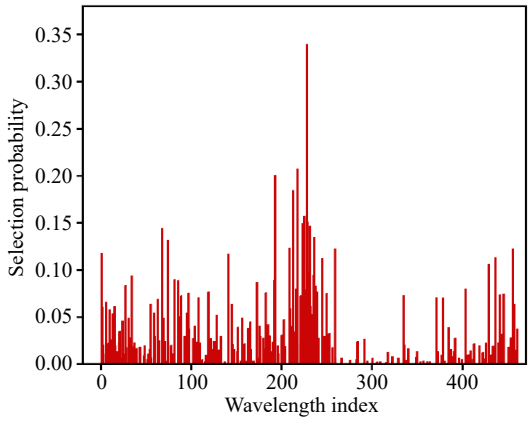

Fig. 5 Firmness feature extraction of RF.

high degree of accuracy in model detection. The CARS and RF algorithms effectively reduced the number of feature variables to less than 5% of the full band (13 and 17 wavelengths, respectively). As shown in Table 2, compared to RW-PLS model, the R_c^2 and R_p^2 are slightly lower but the *RMSEC* and *RMSEP* are larger in the RF-PLS model, indicating that RW-PLS model is superior to the RF-PLS model and eliminating some relevant regions leads to a slightly inferior prediction performance. On the contrary, despite the limited number of relevant feature wavelength chosen by the CARS feature wavelengths extraction method, the R_p^2 of the firmness at 0.8325, with an *RMSEP* of 0.6257. The detection performances of RF-PLS models exhibited slight decreases, whereas those of CARS-PLS models demonstrated improvements. This demonstrates that the PLS model employing the CARS feature wavelength extraction method eliminates regions with low correlation, reduces modeling redundancy significantly, preserves the effective region, and improves efficiency by reducing the time needed. Hence, the CARS feature wavelength extraction method was chosen to extract the characteristic wavelength of apple samples.

Analysis of firmness prediction models

PLS, MLR, HTL, and BPNN models were developed to learn firmness feature of apple using RW and CARS wavelengths. The performance of each model is shown in Table 3. The BPNN model using the feature wavelength by CARS algorithm (CARS-BPNN) obtained the optimum predictive performance, with R_c^2, *RMSEC*, R_p^2, and *RMSEP* of 0.9532, 0.4184, 0.9350, and 0.4654, respectively.

Table 2. Comparison of different feature wavelengths in the calibration set and prediction set.

Model	No. of wavelengths	R_c^2	*RMSEC*	R_p^2	*RMSEP*
RW-PLS	462	0.7862	0.6505	0.7925	0.6537
CARS-PLS	13	0.8484	0.5965	0.8325	0.6257
RF-PLS	17	0.7666	0.6719	0.7480	0.7054

Table 3. Parameter evaluation of models and CARS feature wavelengths for firmness prediction.

Model	Input	R_c^2	*RMSEC*	R_p^2	*RMSEP*
PLS	CARS	0.8484	0.5965	0.8325	0.6257
MLR	CARS	0.8843	0.4994	0.8718	0.5069
HTL	CARS	0.9344	0.4487	0.9254	0.4691
BPNN	CARS	0.9523	0.4184	0.9350	0.4654

To verify the superiority of the BPNN model, various models, and spectral extraction methods were mixed for cross-testing performance, and the confusion matrix. Figure 6 was made according to the evaluation parameters, which showed that the modeling performance of the BPNN model was more effective than the other three modeling methods. The figure illustrates that all 12 models are capable of accurately detecting the firmness of the apple. Furthermore, the overall performance of the model calibration set was found to be marginally superior to that of the prediction set. Nevertheless, the discrepancy was not statistically significant, suggesting that the performances were consistent across the four methods and that there was no major problem with overfitting. The R^2 and *RMSE* of firmness calibration and prediction set of the BPNN model were 0.9523, 0.4184, 0.9350, and 0.4654, respectively. The *RMSEP* of BPNN model was 11.53% lower than that of the other three models, and the R_p^2 was 6.87% higher than that of the other three models.

The RW-PLS, RW-MLR, RW-HTL, and RW-BPNN models exhibited superior calibration performance, as all calibration sets displayed correlation coefficients floating around 0.8. This indicates the existence of both linear and nonlinear correlations between the RW and firmness. The recognition ability of the RW-MLR, RW-HTL, and RW-BPNN models was superior to that of the RW-PLS models, implying that the nonlinear relationship with the RW was pronounced rather than the linear relationship. The RW-BPNN model displayed superior performance versus the other three models, indicating an enhanced capacity for processing both linear and nonlinear relationships.

The CARS-BPNN models' predictive performance was assessed. As can be seen from Fig. 7, which shows scatter plots of the predicted and true firmness of the apple samples, the findings for the CARS-BPNN model exhibited strong prediction and accuracy. The anticipated firmness values also corresponded well with the actual firmness. The tight distribution of the plot's scatterplots around the predicted regression plot suggested that the model could identify an apple's firmness with a high degree of accuracy. Accordingly, the model could be employed to reliably monitor the firmness evolution of the apple.

Conclusions

In this work, 'Fuji' apples were selected as subjects to predict firmness. To optimize the quality of marketable fruit, it is essential to design a rapid, nondestructive technology testing system for pre-market apples. Firmness indicator monitoring is employed to predetermine the quality of apples by a deep learning model. The accuracy of the CARS-BPNN was demonstrated with excellent

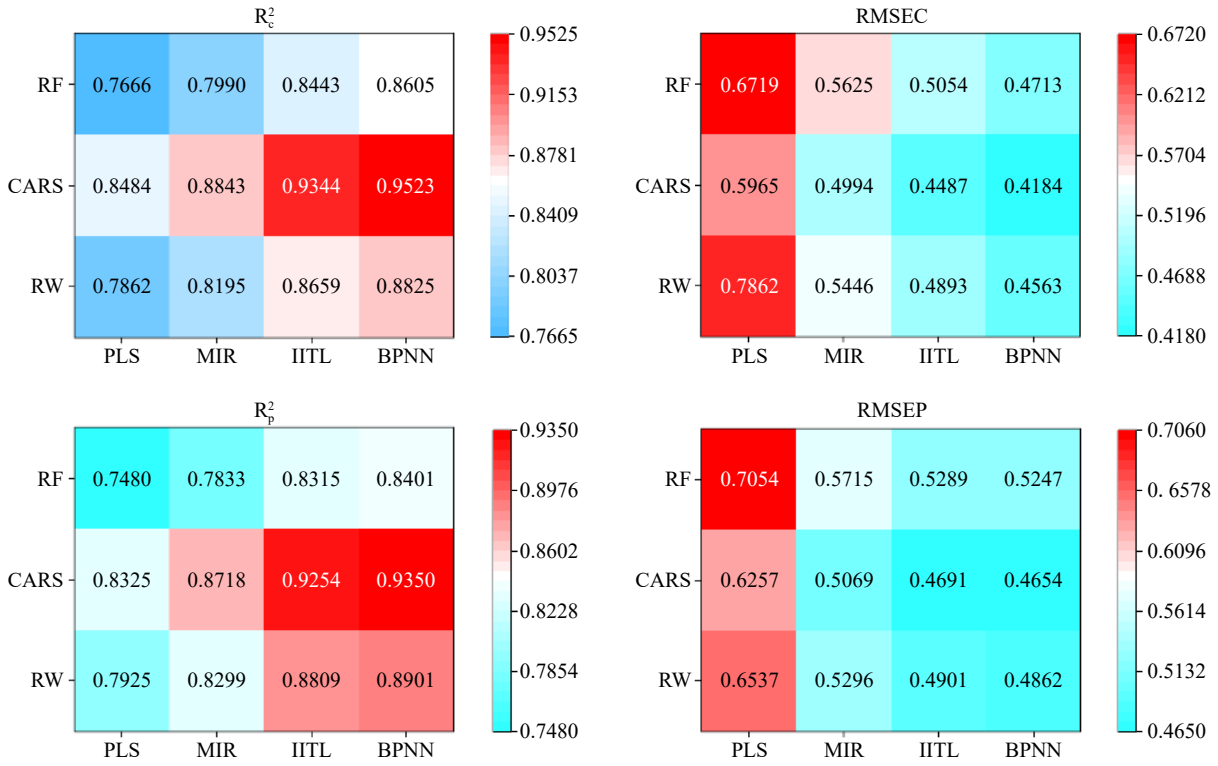

Fig. 6 Matrix heatmap.

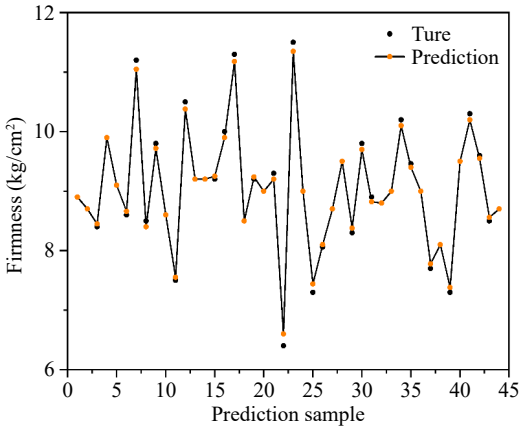

Fig. 7 Line plots of actual vs predicted firmness on the prediction set.

agreement with real experimental values. The cross-validation of different wavelengths and different models was displayed, and the prediction model of apple firmness by CARS-BPNN algorithm is optimum (R_p^2 = 0.9350, R_c^2 = 0.9523, *RMSEP* = 0.4654, *RMSEC* = 0.4184). The results provided some references for other researchers in the field to select pre-processing and feature selection algorithms.

However, there are several potential challenges and limitations to the development and evaluation of deep learning models, including those related to data quality and privacy, the challenge of algorithm selection and optimization, model representability, and other ethical sensitivities. In light of these prospective challenges, and constraints, the subsequent research trajectory for the optimization of the industrialization of fruit quality should be to ascertain methodologies to surmount them. It is recommended that future research on fruit quality assessment based on artificial intelligence prioritize interdisciplinary collaboration, leverage big data and deep learning techniques to enhance prediction accuracy, develop intelligent agriculture systems to optimize harvesting and transportation, and prioritize ethical and privacy considerations to ensure the sustainability and social responsibility of the technology's application.

Author contributions

The authors confirm contribution to the paper as follows: conceptualization: Gao X, Ban Z; project administration: Ban Z; writing – original draft: Li S; writing – review & editing: Li S, Chen Y, Zhang X, Ban Z, Chen C; methodology: Li S, Chen Y, Wang J, Jiang Y, Chen C; investigation: Li S, Zhang X, Jiang Y; formal analysis: Li S, Wang J, Jiang Y, Ban Z; data curation: Li S, Chen Y, Gao X; software: Zhang X, Wang J, Gao X, Jiang Y; resources, supervision: Chen C. All authors reviewed the results and approved the final version of the manuscript.

Data availability

All data generated or analyzed during this study are included in this published article and its supplementary information files.

Acknowledgments

This work was supported by 'Pioneer' and 'Leading Goose' Research and Development Plan Project of Zhejiang Province (2022C04039), Major Scientific Research Achievement Transformation Project of Ningxia Hui Autonomous Region (2023CJE09060), Tianjin Science and Technology Program Project (22ZYCGSN00170, 22ZYCGSN00470), and International Exchanges Funds offered by the Royal Society (No. IEC\NSFC\233076).

Conflict of interest

The authors declare that they have no conflict of interest.

Dates

Received 2 August 2024; Revised 4 December 2024; Accepted 5 December 2024; Published online 16 January 2025

References

1. Wang J, Liu T. 2022. Spatiotemporal evolution and suitability of apple production in China from climate change and land use transfer perspectives. *Food and Energy Security* 11:e386
2. Oyenihi AB, Belay ZA, Mditshwa A, Caleb OJ. 2022. "An apple a day keeps the doctor away": The potentials of apple bioactive constituents for chronic disease prevention. *Journal of Food Science* 87:2291–309
3. Harker FR, Roigard CM, Colonna AE, Jin D, Ryan G, et al. 2024. The relative importance of postharvest eating quality and sustainability attributes for apple fruit: A case study using new sensory-consumer approaches. *Postharvest Biology and Technology* 217:113099
4. Cheng XY, Zhao YY, Xue HL, Bi Y, Sun CC, et al. 2022. Model fit based on the weight loss and texture parameters of MAP cherry tomatoes during storage. *Journal of Food Processing and Preservation* 46:e16204
5. Bejaei M, Stanich K, Cliff MA. 2021. Modelling and classification of apple textural attributes using sensory, instrumental and compositional analyses. *Foods* 10:384–97
6. Yang X, Zhu L, Huang X, Zhang Q, Li S, et al. 2022. Determination of the soluble solids content in korla fragrant pears based on visible and near-infrared spectroscopy combined with model analysis and variable selection. *Frontiers in Plant Science* 13:938162
7. Liu Y, Wu Q, Huang J, Zhang X, Zhu Y, et al. 2021. Comparison of apple firmness prediction models based on non-destructive acoustic signal. *International Journal of Food Science and Technology* 56:6443–50
8. Martínez Gila DM, Navarro Soto JP, Satorres Martínez S, Gómez Ortega J, Gámez García J. 2022. The advantage of multispectral images in fruit quality control for extra virgin olive oil production. *Food Analytical Methods* 15:75–84
9. Wang C, Liu B, Liu L, Zhu Y, Hou J, et al. 2021. A review of deep learning used in the hyperspectral image analysis for agriculture. *Artificial Intelligence Review* 54:5205–53
10. Wesoły M, Przewodowski W, Ciosek-Skibińska P. 2023. Electronic noses and electronic tongues for the agricultural purposes. *Trends in Analytical Chemistry* 164:117082–103
11. Schlie TP, Dierend W, Köpcke D, Rath T. 2022. Detecting low-oxygen stress of stored apples using chlorophyll fluorescence imaging and histogram division. *Postharvest Biology and Technology* 189:111901–09
12. Peng K, Ma W, Lu J, Tian Z, Yang Z. 2023. Application of machine vision technology in citrus production. *Applied Sciences* 13:9334
13. Zhang P, Wang H, Ji H, Li Y, Zhang X, et al. 2023. Hyperspectral imaging-based early damage degree representation of apple: a method of correlation coefficient. *Postharvest Biology and Technology* 199:112309–17
14. Arendse E, Nieuwoudt H, Magwaza LS, Nturambirwe JFI, Fawole OA, et al. 2021. Recent advancements on vibrational spectroscopic techniques for the detection of authenticity and adulteration in horticultural products with a specific focus on oils, juices and powders. *Food and Bioprocess Technology* 14:1–22
15. Shlezinger N, Whang J, Eldar YC, Dimakis AG. 2023. Model based deep learning. *Proceedings of the IEEE* 111:465–99
16. Zhou L, Zhang C, Liu F, Qiu Z, He Y. 2019. Application of deep learning in food: A review. *Comprehensive Reviews in Food Science and Food Safety* 18:1793–811
17. Li S, Song Q, Liu Y, Zeng T, Liu S, et al. 2023. Hyperspectral imaging-based detection of soluble solids content of loquat from a small sample. *Postharvest Biology and Technology* 204:112454
18. Tian Y, Sun J, Zhou X, Yao K, Tang N. 2022. Detection of soluble solid content in apples based on hyperspectral technology combined with deep learning algorithm. *Journal of Food Processing and Preservation* 46:e16414
19. Ma T, Xia Y, Inagaki T, Tsuchikawa S. 2021. Non-destructive and fast method of mapping the distribution of the soluble solids content and pH in kiwifruit using object rotation near-infrared hyperspectral imaging approach. *Postharvest Biology and Technology* 174:111440–47
20. Park B, Shin T, Cho JS, Lim JH, Park KJ. 2023. Improving blueberry firmness classification with spectral and textural features of microstructures using hyperspectral microscope imaging and deep learning. *Postharvest Biology and Technology* 195:112154–64
21. Ragavendra S, Ganguli S, Selvan PT, Nayak MM, Chaudhury S, et al. 2022. Deep learning based dual channel banana grading system using convolution neural network. *Journal of Food Quality* 2022:6050284
22. Xiang Y, Chen Q, Su Z, Zhang L, Chen Z, et al. 2022. Deep learning and hyperspectral images based tomato soluble solids content and firmness estimation. *Frontiers in Plant Science* 13:860656–66
23. Xu M, Sun J, Yao K, Cai Q, Shen J, et al. 2022. Developing deep learning based regression approaches for prediction of firmness and pH in kyoho grape using Vis/NIR hyperspectral imaging. *Infrared Physics and Technology* 120:104003–12
24. Liu P, Zhang P, Ni F, Hu Y. 2021. Feasibility of nondestructive detection of apple crispness based on spectroscopy and machine vision. *Journal of Food Process Engineering* 44:13802
25. Shao Y, Ji S, Xuan G, Wang K, Xu L, et al. 2024. Soluble solids content monitoring and shelf life analysis of winter jujube at different maturity stages by Vis-NIR hyperspectral imaging. *Postharvest Biology and Technology* 210:112773–80
26. Kim HJ, Baek JW, Chung K. 2021. Associative knowledge graph using fuzzy clustering and min-max normalization in video contents. *IEEE Access* 9:74802–16
27. Siino M, Tinnirello I, La Cascia M. 2024. Is text preprocessing still worth the time? A comparative survey on the influence of popular preprocessing methods on transformers and traditional classifiers. *Information Systems* 121:102342
28. Liu HL, Yu CH, Wan LC, Qin SJ, Gao F, et al. 2022. Quantum mean centering for block-encoding-based quantum algorithm. *Physica A: Statistical Mechanics and its Applications* 607:128227
29. Sohn SI, Pandian S, Oh YJ, Zaukuu JLZ, Na CS, et al. 2022. Vis-NIR spectroscopy and machine learning methods for the discrimination of transgenic *Brassica napus* L. and their hybrids with *B. juncea*. *Processes* 10:240
30. Butt UM, Letchmunan S, Ali M, Hassan FH, Baqir A, et al. 2021. Machine learning based diabetes classification and prediction for healthcare applications. *Journal of Healthcare Engineering* 2021:9930985
31. Figueiredo NS, Ferreira LHC, Dutra OO. 2019. An approach to savitzky-golay differentiators. *Circuits Systems and Signal Processing* 38:4369–79
32. Endut R, Sabri MSA, Aljunid SA, Ali N, Laili AR, et al. 2023. Prediction of potassium (K) content in soil analysis utilizing near-infrared (NIR) spectroscopy. *Journal of Advanced Research in Applied Sciences and Engineering Technology* 33:92–101
33. Gao Q, Wang P, Niu T, He D, Wang M, et al. 2022. Soluble solid content and firmness index assessment and maturity discrimination of *Malus micromalus Makino* based on near-infrared hyperspectral imaging. *Food Chemistry* 370:131013
34. Xuan W, Wang Y. 2021. Competitive adaptive reweighted sampling method for fault detection. *Journal of Physics: Conference Series* 1820:012078
35. Sun J, Yang W, Feng M, Liu Q, Kubar M. 2020. An efficient variable selection method based on random frog for the multivariate calibration of NIR spectra. *RSC Advances* 10:16245–53
36. Meng Q, Shang J, Huang R, Zhang Y. 2021. Determination of soluble solids content and firmness in plum using hyperspectral imaging and chemometric algorithms. *Journal of Food Process Engineering* 44:e13597
37. Chen Y, Jiang X, Liu Q, Wei Y, Wang F, et al. 2024. A hyperspectral imaging technique for rapid non-destructive detection of soluble solid content and firmness of wolfberry. *Journal of Food Measurement and Characterization* 18:7927–41
38. Tang N, Sun J, Yao K, Zhou X, Tian Y, et al. 2021. Identification of *Lycium barbarum* varieties based on hyperspectral imaging technique and competitive adaptive reweighted sampling-whale optimization algorithm-support vector machine. *Journal of Food Process Engineering* 44:e13603
39. Xia Z, Yang J, Wang J, Wang S, Liu Y. 2020. Optimizing rice near-infrared models using fractional order savitzky–golay derivation (FOSGD) combined with competitive adaptive reweighted sampling (CARS). *Applied Spectroscopy* 74:417–26

40. Meng Q, Tan T, Feng S, Wen Q, Shang J. 2024. Prediction and visualization map for physicochemical indices of kiwifruits by hyperspectral imaging. *Frontiers in Nutrition* 11:1364274
41. Xing Z, Du C, Shen Y, Ma F, Zhou J. 2021. A method combining FTIR-ATR and raman spectroscopy to determine soil organic matter: Improvement of prediction accuracy using competitive adaptive reweighted sampling (CARS). *Computers and Electronics in Agriculture* 191:106549
42. Yang B, Li X, Wu L, Chen Y, Zhong F, et al. 2022. Citrus huanglongbing detection and semi-quantification of the carbohydrate concentration based on micro-FTIR spectroscopy. *Analytical and Bioanalytical Chemistry* 414:6881–97
43. Chen S, Lou F, Tuo Y, Tan S, Peng K, et al. 2023. Prediction of soil water content based on hyperspectral reflectance combined with competitive adaptive reweighted sampling and random frog feature extraction and the back-propagation artificial neural network method. *Water* 15:2726
44. Gorzelany J, Belcar J, Kuźniar P, Niedbała G, Pentoś K. 2022. Modelling of mechanical properties of fresh and stored fruit of large cranberry using multiple linear regression and machine learning. *Agriculture* 12:200
45. Luo Y, Wen Y, Liu T, Tao D. 2019. Transferring knowledge fragments for learning distance metric from a heterogeneous domain. *IEEE Transactions on Pattern Analysis and Machine Intelligence* 41:1013–26
46. Elsherbiny O, Fan Y, Zhou L, Qiu Z. 2021. Fusion of feature selection methods and regression algorithms for predicting the canopy water content of rice based on hyperspectral data. *Agriculture* 11:51–71
47. Ciccoritti R, Paliotta M, Amoriello T, Carbone K. 2019. FT-NIR spectroscopy and multivariate classification strategies for the postharvest quality of green-fleshed kiwifruit varieties. *Scientia Horticulturae* 257:108622–31